RF-Based Human Activity Recognition: A Non-Stationary Channel Model Incorporating the Impact of Phase Distortions*

Alireza Borhani and Matthias Pätzold

Faculty of Engineering and Science, University of Agder, P.O. Box 509, 4898 Grimstad, Norway {alireza.borhani, matthias.paetzold}@uia.no
http://www.mcg.uia.no

Abstract. This paper proposes a non-stationary channel model that captures the impact of the time-variant (TV) phase distortion caused by hardware imperfections. The model allows for studying the spectrogram of in-home radio channels influenced by walking activities of the home user under realistic non-stationary propagation conditions. The resolution of the spectrogram is investigated for the von-Mises distribution of the phase distortion. It is shown that high-entropy distributions considerably mask fingerprints of the user activity on the spectrogram of the channel. For an orthogonal frequency-division multiplexing (OFDM) system, a computationally simple method for mitigating the undesired phase rotation is proposed. Both theoretical and simulation results confirm that the proposed method significantly reduces the impact of the phase distortion, allowing us to retrieve the desired spectrogram imprinted by the activity of the home user. The results of this paper are useful for the development of software-based radio frequency (RF)-based activity recognition systems.

Keywords: RF-based human activity recognition · non-stationary channel modelling · spectrogram analysis · phase distortion.

1 Introduction

The World Health Organization (WHO) states that the global average life expectancy increased by 5.5 years between 2000 and 2016, the fastest increase since the 1960s [1]. With such a trend, more and more seniors are expected to live a longer independent life. To assure the quality of independent living, in-home activity monitoring systems, such as video cameras, vision sensors, wearable devices, and smart floors, are emerging. These systems send healthcare information, such as daily activity information and multimodal bio-sensors data, to remote caregivers, who act accordingly. These systems are often expensive, but more importantly, intrusive in terms of privacy and comfort of the home user.

* This work was supported by the WiCare Project through the Research Council of Norway under Grant 261895/F20.

Such drawbacks have triggered a so-called radio frequency (RF)-based activity recognition approach, according to which no user involvement in the monitoring mechanism is required.

In this approach, a transmit antenna emits radio waves throughout the in-home propagation area, while a receive antenna receives the waves reflected off the body of the home occupant, and thus collecting fingerprints of the user activity in the environment. The new approach indeed allows for a passive indoor radar solution without the active participation of the users and without compromising their privacy. The collected radio waves are imprinted quite differently depending on the type of the activity. Therefore, sophisticated recognition algorithms and machine learning methods are required to distinguish activities from each other. The number of proposed activity recognition systems is increasing. Employing principles of radar systems [3, 14], ultrawide band sensors [8], received signal strength indicator (RSSI) [7], and the channel state information (CSI) [4, 9, 18–20] are the main levers for the development of activity recognition systems. A comprehensive survey of the existing literature on the RF-based activity recognition can be found in, e.g., [5].

To the best knowledge of authors, all the proposed activity recognition systems have been developed using an experimental design approach, which is very time-consuming and costly. Often, numerous repetitions of the measurement are required in distinct experimental setups, such that machine learning algorithms can be sufficiently trained. However, a software-based design approach, in which channel models/simulators generate numerous datasets under different propagation conditions and different mobility patterns in a very short time, can save time and money compared to conducting a large number of real experiments. The data can then be used to train and to test detection algorithms. The software-based design approach has been very rarely, if at all, addressed in the literature. The channel model proposed in [2] is an exception that can generate experimentally verifiable complex channel gain data. However, the model in [2] does not capture the time-variant (TV) phase distortion, which in practice exists due to the hardware imperfection, such as carrier frequency offset (CFO) and sampling frequency offset (SFO). In fact, the undesired phase rotation caused by the imperfection of a device, e.g., Intel NIC 5300, significantly interferes with the desired phase rotation caused by the human activities, which ultimately reduces the performance of detection algorithms. Coping with the phase distortion has been a challenge for most of the literature listed above, as well as [6, 16, 17].

In this paper, we propose a non-stationary channel model that incorporates the effect of phase distortion in terms of a stochastic process. To study the time-frequency distribution of the channel, the spectrogram of the complex channel gain is computed. The spectrogram provides useful information about the variations of Doppler frequency components in time, allowing us to track the human walking pattern. The impact of different distributions of the phase distortion on the spectrogram of the complex channel gain is analyzed, showing that the expected observations are considerably spoiled when the undesired phase rotation is integrated into the model. To mitigate the impact of phase distor-

tion, a computationally efficient method based on the principles of orthogonal frequency-division multiplexing (OFDM) systems is proposed. It is shown that the proposed method retrieves the desired spectrogram imprinted by the activity of the user.

The remainder of this paper is organized as follows. Sections 2 and 3 describe the in-home propagation scenario and present the phase distortions, respectively. The complex channel gain and its time-frequency distribution are presented in Sections 4 and 5. Section 6 proposes the distortion mitigation technique. Simulation results are presented in Section 7. Finally, Section 8 concludes the paper.

2 Propagation Scenario

With reference to Fig. 1, a fixed-to-fixed propagation scenario is assumed in which an omnidirectional transmitter (Tx) antenna is placed on the floor and an omnidirectional receiver (Rx) antenna is mounted on the ceiling of the room. The position of the Tx (Rx) is denoted by (x^T, y^T, z^T) $((x^R, y^R, z^R))$, while the positions of N_F fixed scatterers (black stars in Fig. 1) are given by $(x^S_{n_F}, y^S_{n_F}, z^S_{n_F})$, where $n_F = 1, 2, ..., N_F$. It is assumed that the line-of-sight (LOS) between the Tx and the Rx is blocked.

A cluster of N_M moving scatterers S^M_n $(n_M = 1, 2, ..., N_M)$ accounts for the human body parts, such as the head, hands, and legs. The random trajectory approach in [2] is used to model a moving person, starting from (x_s, y_s, z_s) and terminating at a predefined destination point (x_d, y_d, z_d). In particular, a realization of the random trajectory (based on the first primitive of Brownian fields) gives a set of triples (x_l, y_l, z_l), where l denotes the position index (or equivalently t represents the corresponding time). It is assumed that the random bridge is fully established, while the drift to the destination point exists. For simplicity reasons, the horizontal displacement of the path from the shortest path is assumed to be zero. A single realization of the random trajectory model generates a master trajectory $\mathcal{T}$, explaining the spatial behavior of each body part if it is shifted to its corresponding starting point (x_s, y_s, z_s). The temporal features of the motion are added to the spatial trajectory model by employing horizontal and vertical speed vectors (similar to those used in [2]), describing the temporal behaviour of the body parts along the path (see Sec. 7 for details).

It is assumed that a plane wave emitted from the Tx with an azimuth angle-of-departure (AOD) $\alpha^T_n(t)$ and an elevation AOD $\beta^T_n(t)$ reaches the Rx with an azimuth angle-of-arrival (AOA) $\alpha^R_n(t)$ and an elevation AOA $\beta^R_n(t)$ after a single bounce with the nth scatterer $S^{(.)}_n$. Note that in case of N_F fixed scatterers S^F_n, none of those angles change in time, but they change in time according to the trajectory of the N_M moving scatterers S^M_n. It is also assumed that the reverberation effect between the fixed and moving scatterers does not exist.

Furthermore, it is assumed that the communication is established through K subcarriers of an OFDM WiFi system. This corresponds to the principles of a typical commodity WiFi system, such as Intel NIC 5300, which has been the core tool of many experimental studies in this field, e.g., [4].

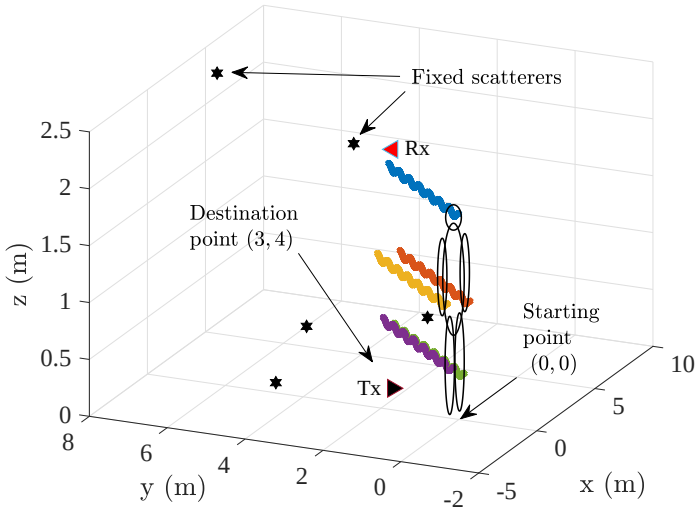

Fig. 1. The schema of an in-home propagation area, illustrating the trajectories of a person's head, arms, and legs, if the person walks from the starting point $(0, 0)$ to the destination point (3,4).

3 Phase Distortions

In practice, the phase of the received multipath components is often determined by two main factors, namely the phase shift caused by the propagation delay and the phase shift caused by the device characteristics (imperfection). The propagation delays and the corresponding phase shifts remain constant in time if the environment is stationary. However, if some objects (herein, the user) starts moving, the corresponding propagation delay and thus the associated phase vary in time. Such variations carry fingerprints of the user activities in the propagation area, which can be used for activity recognition purposes. With this token, the phase rotation caused by a change of the propagation delay is called the *desired phase rotation*.

In contrast, device imperfections result in an *undesired phase rotation* that can hardly be characterized, mainly because it is a superposition of several phase shifts originating from different sources [6]. The carrier frequency offset, sampling frequency offset, packet boundary offset, and the phase-locked loop offset are the main hardware-related sources of phase distortion in experimental studies [15, 17, 18, 20]. The undesired phase distortion $\boldsymbol{\Phi}_1^{(k)}(t)$ changes across both the OFDM subcarrier index k and the time variable t, making coping more challenging. Let us assume $H_1^{(k)}(f, t)$ denotes the channel transfer function (CTF) associated with the kth subcarrier of an OFDM WiFi system with phase dis-

tortions. This function can then be written as $H_1^{(k)}(f,t) = \tilde{H}^{(k)}(f,t)e^{j\boldsymbol{\Phi}_1^{(k)}(t)}$, in which $\tilde{H}^{(k)}(f,t)$ is the corresponding undistorted CTF.

In the literature, there exists a number of phase sanitization techniques[1], transforming the distorted CTF $H_1^{(k)}(f,t)$ to the calibrated CTF $H^{(k)}(f,t) = H_1^{(k)}(f,t)e^{-j\Phi_2{}^{(k)}(t)} = \tilde{H}^{(k)}(f,t)e^{j(\boldsymbol{\Phi}_1^{(k)}(t)-\Phi_2{}^{(k)}(t))}$, where $\Phi_2{}^{(k)}(t)$ accounts for the phase shift originated from the employed sanitization technique. However, these techniques cannot fully retrieve the desired phase rotation [6], meaning that the residual phase $\boldsymbol{\Phi}^{(k)}(t) = \boldsymbol{\Phi}_1^{(k)}(t) - \Phi_2{}^{(k)}(t)$ still distorts the time-frequency observations.

On the other hand, the randomness of the phase distortion adds a significant level of uncertainty to the residual phase rotation $\boldsymbol{\Phi}^{(k)}(t)$, spoiling the performance of activity recognition algorithms based on the time-frequency distribution of the channel. Therefore, it is of great importance to understand the impact of the undesired phase rotation $\boldsymbol{\Phi}^{(k)}(t)$ on the spectrogram of the complex channel gain.

In this paper, the undesired (residual) phase rotation $\boldsymbol{\Phi}^{(k)}(t)$ is modelled by a stochastic process following the von-Mises distribution, i.e.,

$$p_{\boldsymbol{\Phi}^{(k)}(t)}(\Phi|\,\Phi_0,\kappa) = \frac{e^{\kappa\cos(\Phi-\Phi_0)}}{2\pi I_0(\kappa)} \tag{1}$$

where Φ_0 and κ are the parameters of the circular distribution, while $I_0(.)$ denotes the zeroth-order modified Bessel function. The values of the undesired phase rotation across both subcarrier k and time t are independent outcomes of the distribution function in (1). The reason for this choice is the flexibility of the von-Mises distribution, ranging from the uniform distribution for $\kappa = 0$, over approximating the Gaussian distribution, and up to very concentrated distributions for large values of κ. Indeed, the von-Mises distribution allows us to assess the impact of different distortion entropies on the spectrogram of the channel.

4 Non-Stationary Channel Model

Given the propagation scenario in Sec. 2, the complex channel gain $\boldsymbol{\mu}^{(k)}(t)$ associated with the kth subcarrier equals the CTF $H^{(k)}(f,t)$ of the same subcarrier frequency $f^{(k)}$. It follows $\boldsymbol{\mu}^{(k)}(t) = \tilde{\boldsymbol{\mu}}^{(k)}(t)e^{j\boldsymbol{\Phi}^{(k)}(t)}$, in which $\tilde{\boldsymbol{\mu}}^{(k)}(t)$ is the undistorted complex channel gain and $\boldsymbol{\Phi}^{(k)}(t)$ represents the TV residual phase distortion discussed in Sec. 3. Under NLOS propagation conditions, the non-distorted complex channel gain $\tilde{\boldsymbol{\mu}}^{(k)}(t)$ is modelled by a process representing the sum $\boldsymbol{\mu}_F$ of the scattered components due to the N_F fixed scatterers and the sum $\boldsymbol{\mu}_M(t)$ of TV components due to the N_M moving scatterers. It follows

[1] A known example is to compensate the phase rotation by linearly removing the mean and the slope of the measured CSI phase [16, 17]. This technique removes parts of the desired CSI, but more importantly has no physical justification [6].

$$\mu^{(k)}(t) = \tilde{\boldsymbol{\mu}}^{(k)}(t) e^{j\boldsymbol{\Phi}^{(k)}(t)} = \left(\tilde{\boldsymbol{\mu}}_F + \tilde{\boldsymbol{\mu}}_M^{(k)}(t)\right) e^{j\boldsymbol{\Phi}^{(k)}(t)}$$
$$= \left(\sum_{n_F=1}^{N_F} c_{n_F} e^{j\boldsymbol{\phi}_{n_F}} + \sum_{n_M=1}^{N_M} c_{n_M}(t) e^{j\boldsymbol{\phi}_{n_M}^{(k)}(t, \tau'_{n_M})} \right) e^{j\boldsymbol{\Phi}^{(k)}(t)} \quad (2)$$

in which $\boldsymbol{\phi}_{n_M}^{(k)}(t, \tau'_{n_M}) = \boldsymbol{\phi}_{n_M} - 2\pi f_0^{(k)} \tau'_{n_M}(t)$. In (2), the propagation path gain $c_{n_{(.)}}(t)$ is given by a negative path loss exponent γ applied to the total travelling distance $D_{n_{(.)}}(t)$ of the $n_{(.)}$th plane wave, i.e., $c_{n_{(.)}}(t) = C D_{n_{(.)}}^{-\gamma}(t)$, where the constant C accounts for the Tx(Rx) antenna gain, transmission power, and the wave length (see [11,12]). The total travelling distance $D_{n_{(.)}}(t)$ can be readily calculated by using the known coordinates of the trajectory $\mathcal{T}$ and those of the Tx/Rx. The constant phase shifts $\boldsymbol{\phi}_{n_F}$ and $\boldsymbol{\phi}_{n_M}$ account for the physical interaction of the emitted wave with the n_Fth fixed scatterer and n_Mth moving scatterer, respectively. These two shifts are assumed to be uniformly and independently distributed random variables ranging from $-\pi$ to π [13, p. 47]. The propagation delay $\tau'_{(.)}(t)$ is proportional to the propagation path length $D_{n_{(.)}}(t)$, and is also related to the Doppler frequency $f_{(.)}^{(k)}(t)$ via (without proof) $f_{(.)}^{(k)}(t) = -f_0^{(k)} \dot{\tau}'_{(.)}(t)$, where $\dot{\tau}'_{(.)}(t)$ represents the derivation of the TV delay $\tau'_{(.)}(t)$ with respect to time t. From the latter relationship, it is straightforward to confirm that fixed scatterers contribute to the time-frequency distribution of the channel with zero Doppler shifts, as $\dot{\tau}'_{n_F}(t) = \dot{\tau}'_{n_F} = 0$.

5 Spectrogram Analysis

A practical approach to study the time-frequency distribution of the channel is to perform a spectrogram analysis on the complex channel gain process $\mu^{(k)}(t)$ (a sample function of the process $\boldsymbol{\mu}^{(k)}(t)$ in (2)). To this aim, one first needs to multiply $\mu^{(k)}(t)$ with a sliding window function $w(t' - t)$, i.e.,

$$x_\mu^{(k)}(t', t) = \mu^{(k)}(t) w(t' - t) \quad (3)$$

where $w(t)$ is a positive even function with normalized energy. In this paper, a Gaussian function is used to window the main signal $\mu^{(k)}(t)$. Applying the Fourier transform to the windowed signal $x_\mu^{(k)}(t', t)$ with respect to t' gives then the short-time Fourier transform (STFT)

$$X_\mu^{(k)}(f, t) = \int_{-\infty}^{\infty} x_\mu^{(k)}(t', t) e^{-j2\pi f t'} dt' \quad (4)$$

of the original signal $\mu^{(k)}(t)$. The spectrogram $S_X^{(k)}(f, t)$ is then defined as the squared magnitude of the STFT $X_\mu^{(k)}(f, t)$, i.e., $S_{X_\mu}^{(k)}(f, t) = \left| X_\mu^{(k)}(f, t) \right|^2$.

6 Distortion Mitigation Method

The STFT $X^{(k)}(f,t)$ of the distorted complex channel gain $\mu^{(k)}(t)$ suffers from interfering terms, which can be analytically formulated as

$$\begin{aligned} X_{\mu}^{(k)}(f,t) &= \int_{-\infty}^{\infty} x_{\tilde{\mu}}^{(k)}(t',t) e^{j\Phi^{(k)}(t')} e^{-j2\pi\, ft'} dt' \\ &= \int_{-\infty}^{\infty} x_{\tilde{\mu}}^{(k)}(t',t) e^{-j2\pi\, ft'} \left(\sum_{l=0}^{\infty} \frac{(j\Phi^{(k)}(t'))^l}{l!} \right) dt' \\ &= X_{\tilde{\mu}}^{(k)}(f,t) + I_1(f,t) + jI_2(f,t) \end{aligned} \tag{5}$$

where $X_{\tilde{\mu}}^{(k)}(f,t)$ represents the desired STFT, while $I_1(f,t)$ and $I_2(f,t)$ stand for the interfering terms caused by the elements $l = 1, 2, ..., \infty$ of the Maclaurin series of the phase distortion. Consequently, the spectrogram $S_{X_\mu}^{(k)}(f,t)$ of $\mu^{(k)}(t)$ includes complex-valued interfering terms that change not only in time t, but also in frequency f.

To mitigate the impact of such undesired components, a simple (computationally inexpressive) approach is to first average over K distorted complex channel gain $\mu^{(k)}(t)$, and then to apply the spectrogram analysis on the average $\bar{\mu}(t)$. The theoretical justification of this technique is that $\bar{\mu}(t) = E\{\mu^{(k)}(t)\}$ equals to $E\{\tilde{\mu}^{(k)}(t) e^{j\Phi^{(k)}(t)}\}$, which after some mathematical manipulations can be approximated by $\tilde{\mu}^{(.)}(t) \frac{I_1(\kappa)}{I_0(\kappa)} e^{j\Phi_0}$, where κ and Φ_0 are the parameters of the von-Mises distribution describing the phase distortion $\Phi^{(k)}(t)$ (see Sec. 3), and $I_1(.)$ denotes the modified Bessel function of the first kind. The STFT $X_{\bar{\mu}}(f,t)$ of the averaged complex channel gain $\bar{\mu}(t)$ can then be computed as follows

$$\begin{aligned} X_{\bar{\mu}}(f,t) &= \int_{-\infty}^{\infty} \bar{\mu}(t') w(t',t) e^{-j2\pi\, ft'} dt' \\ &\approx \frac{I_1(\kappa)}{I_0(\kappa)} e^{j\Phi_0} \int_{-\infty}^{\infty} |\tilde{\mu}^{(.)}(t')| e^{j\measuredangle \tilde{\mu}^{(.)}(t)} w(t',t) e^{-j2\pi\, ft'} dt' \\ &= \frac{I_1(\kappa)}{I_0(\kappa)} e^{j\Phi_0} X_{\tilde{\mu}}^{(.)}(f,t). \end{aligned} \tag{6}$$

From the equation above, it can be concluded that $X_{\bar{\mu}}(f,t)$ is a scaled version of the desired STFT $X_{\tilde{\mu}}^{(k)}(f,t)$, where the scaling factor $I_1(\kappa)e^{j\Phi_0}/I_0(\kappa)$ changes neither in time t, nor in frequency f. Therefore, the corresponding spectrogram $S_{X_{\bar{\mu}}}(f,t)$ is also a scaled, yet non-interfered, version of the desired spectrogram $S_{X_{\tilde{\mu}}}^{(.)}(f,t)$. It can be shown that the proposed technique does not mitigate the impact of the phase distortion if the undesired phase follows an absolutely uniform distribution, i.e., if $\kappa = 0$.

7 Simulation Results

The central frequency $f_0 = 5.32\,\text{GHz}$ (associated with Channel 64) of an OFDM WiFi system is considered. The number of $K = 30$ equally spaced OFDM subcar-

riers around this central frequency has been generated. The Tx and Rx antennas are assumed to be placed on the floor and the ceiling of the room at a height of 0.1 m and 2.2 m, respectively (see Fig. 1). The free-space path loss exponent has been set to $\gamma = 2$, which matches our single-bounce scattering scenario, while the constant C has been set to 1. A cluster of $N_M = 5$ moving scatterers, accounting for the head, hands, and legs of the person, as well as a number of $N_F = 5$ fixed scatterers are considered to be present in the propagation environment. The height H of the person is assumed to be 178 cm. It is supposed that the user starts walking from the origin $(x_s, y_s) = (0\,\text{m}, 0\,\text{m})$ of the Cartesian coordinates to reach the preplanned destination point $(x_d, y_d) = (3\,\text{m}, 4\,\text{m})$ via a single realization of the 3D random trajectory $\mathcal{T}$. The user accelerates from a zero speed to a constant vertical (horizontal) walking speed of 0.1 m/s (1 m/s), followed by a deceleration to a zero speed when approaching the destination point. A Gaussian window of size $\sigma_\omega = 50$ ms has been used in the spectrogram analysis.

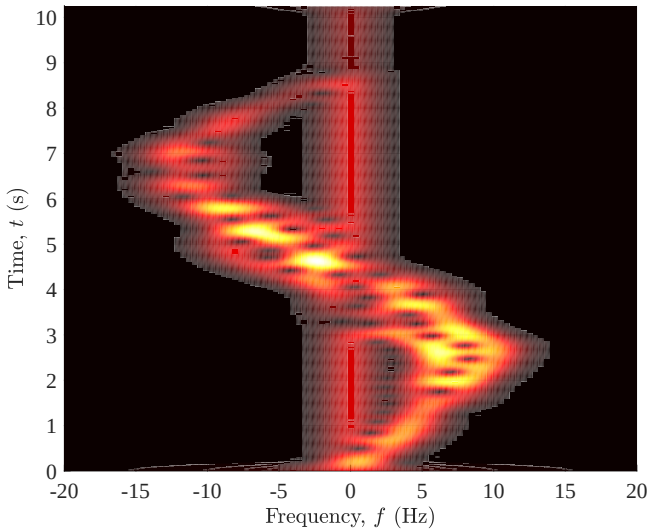

Fig. 2. The spectrogram $S^{(1)}_{X_{\tilde{\mu}}}(f,t)$ of the non-distorted complex channel gain $\tilde{\mu}^{(1)}(t)$ associated with the walking scenario.

Fig. 2 displays the spectrogram $S^{(1)}_{X_{\tilde{\mu}}}(f,t)$ of the non-distorted complex channel gain $\tilde{\mu}^{(1)}(t)$ associated with the walking scenario above. The illustrated spectrogram $S^{(1)}_{X_{\tilde{\mu}}}(f,t)$ provides a non-distorted estimation of TV Doppler frequency components, representing our benchmark for the time-frequency observation associated with the first OFDM subcarrier. For the first three seconds, the Doppler shifts increase from zero (initial stop) to about 12 Hz, confirming the initial ac-

celeration of the user for a normal walk. As the user approaches the vicinity of the RX/TX, the Doppler shifts decrease because the direction of motion becomes almost perpendicular to the direction of arrival. This trend continues almost to the middle of the path, from where the user starts leaving the transceiver, indicated by increasing Doppler frequency shifts towards negative values. For $t > 7$, the Doppler components start vanishing, as the person starts decelerating to a zero speed. The oscillatory behavior of the frequency components is caused by the sinusoidal variations of the user's height within a normal walk process. The time-invariant zero frequency components are due to the presence of fixed scatterers in the propagation environment, while the small frequency spread around $f = 0\,\text{Hz}$ is caused by interfering cross-terms as the artefact of the spectrogram analysis [10]. In a nutshell, the phase rotation caused by the walking activity of the user shapes the spectrogram into a clean S-pattern (see Fig. 2)[2].

Fig. 3 exhibits the spectrogram $S^{(1)}_{X_\mu}(f,t)$ of the distorted complex channel gain $\mu^{(1)}(t)$ for the same walking scenario and for four different values of κ. In

[2] The spectrogram associated with the other OFDM subcarriers is also imprinted with a similar $S-$pattern.

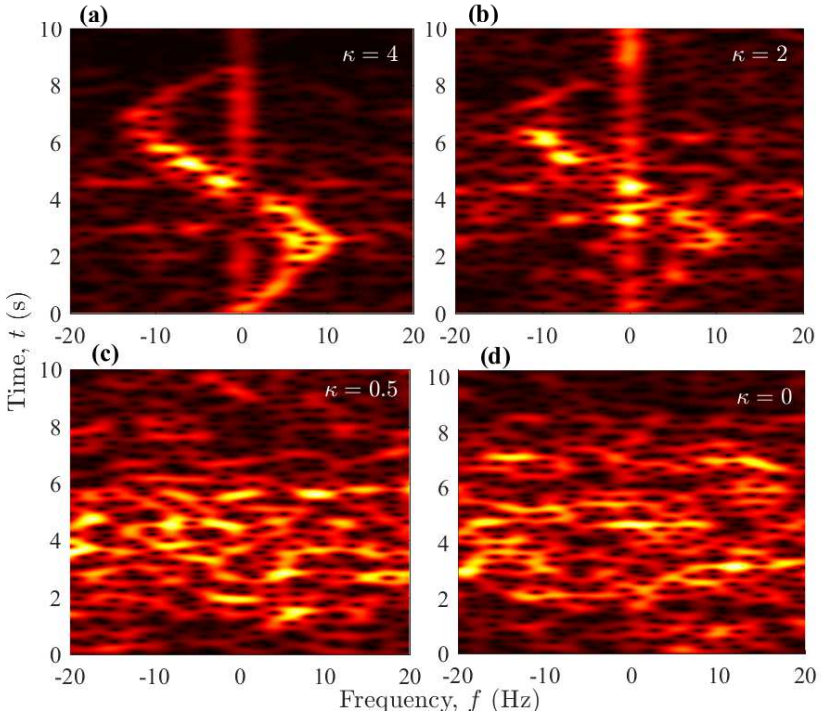

Fig. 3. The spectrogram $S^{(1)}_{X_\mu}(f,t)$ of the distorted complex channel gain $\mu^{(1)}(t)$ for $\Phi_0 = 0$ and (a) $\kappa = 4$, (b) $\kappa = 2$, (c) $\kappa = 0.5$, and (d) $\kappa = 0$.

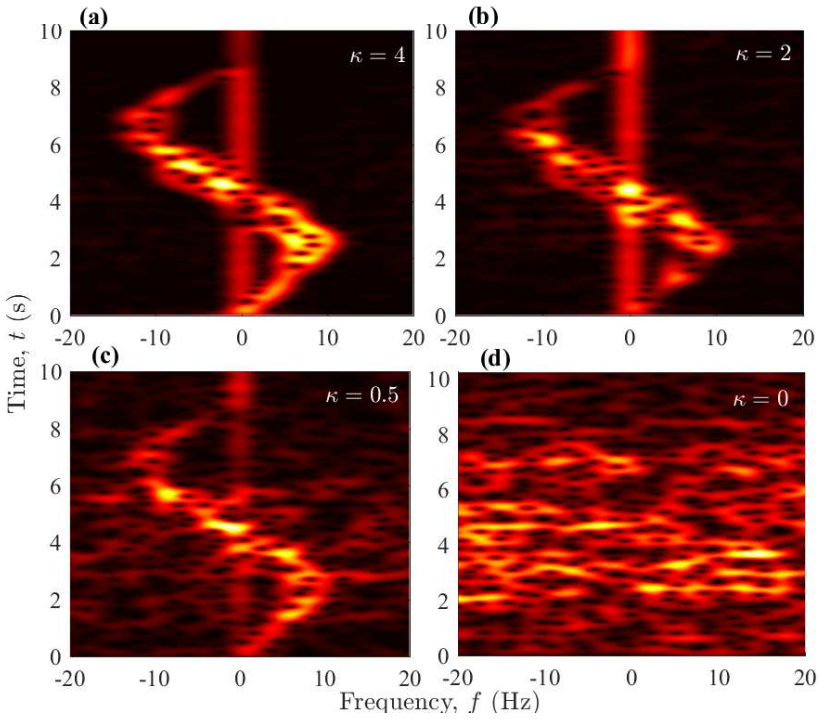

Fig. 4. The spectrogram $S_{X_{\bar{\mu}}}(f,t)$ of the averaged complex channel gain $\bar{\mu}(t)$ for $\Phi_0 = 0$ and (a) $\kappa = 4$, (b) $\kappa = 2$, (c) $\kappa = 0.5$, and (d) $\kappa = 0$.

all subfigures, one can observe that the expected S-pattern is interfered by the frequency contributions originating from the phase distortion. This interference increases if the value of κ decreases. If the phase distortion approaches the uniform distribution, i.e., if $\kappa = 0$, no signature of the desired frequency components can be identified in the plot. For small values of κ, the $S-$pattern in the spectrogram of the channel is hardly distinguishable, while higher values of κ allow for the appearance of the expected pattern. This can be attributed to the fact that higher values of κ result in more concentrated phase distortions with more distinguishable fingerprints in the spectrogram.

Fig. 4 demonstrates the spectrogram $S_{X_{\bar{\mu}}}(f,t)$ of the averaged complex channel gain $\bar{\mu}(t)$ for the same walking scenario and for four different values of κ. This set of figures is one-to-one comparable with those of the previous set shown in 3. As can be observed, the proposed mitigation technique can considerably reduce the interference caused by the phase distortion, so that the $S-$pattern can be restored as the original contribution of the walking person to the time-frequency distribution of the channel. The quality of the proposed sanitization technique decreases if κ decreases. For $\kappa = 0$, the proposed algorithm cannot sanitize the spectrogram of the channel any longer. Theoretically, it can be shown that a

pure uniform distribution of the phase distortion over time completely fades the desired spectrogram $S^{(.)}_{X_{\tilde{\mu}}}(f,t)$. However, an interesting feature of the proposed mitigation scheme is that even a slightly concentrated distribution of the phase distortion, e.g., if $\kappa = 0.5$, allows us to restore the expected $S-$pattern, as can be confirmed in Fig. 4(c).

8 Conclusion

A non-stationary channel model incorporating the impact of phase distortion caused by device imperfections has been developed in this paper. It has been shown that the phase distortion adds significant interference to the time-frequency distribution of the channel. A distortion mitigation technique based on the principles of OFDM systems was proposed. It has been shown that the proposal is robust with respect to the entropy of the distortion distribution. The experimental verification of the proposed method is a topic of future studies.

References

1. Department of Ageing and Life Course: WHO global report on falls prevention in older age, Geneva, Switzerland (2007)
2. Borhani, A., Pätzold, M.: A non-stationary channel model for the development of non-wearable radio fall detection systems. IEEE Transactions on Wireless Communications **17**(11), 7718–7730 (2018)
3. Erol, B., Amin, M.G., Boashash, B.: Range-Doppler radar sensor fusion for fall detection. In: 2017 IEEE Radar Conference (RadarConf). pp. 0819–0824 (May 2017). https://doi.org/10.1109/RADAR.2017.7944316
4. Halperin, D., Hu, W., Sheth, A., Wetherall, D.: Tool release: Gathering 802.11n traces with channel state information. ACM SIGCOMM Computer Communication Review **41**(1), 53–53 (Jan 2011)
5. Jiang, H., Cai, C., Ma, X., Yang, Y., Liu, J.: Smart Home Based on WiFi Sensing: A Survey. IEEE Access **6**, 13317–13325 (2018). https://doi.org/10.1109/ACCESS.2018.2812887
6. Keerativoranan, N., Haniz, A., Saito, K., Takada, J.: Mitigation of CSI temporal phase rotation with B2B calibration method for fine-grained motion detection analysis on commodity Wi-Fi devices. Sensors **18**(11) (Nov 2018). https://doi.org/10.3390/s18113795
7. Kianoush, S., Savazzi, S., Vicentini, F., Rampa, V., Giussani, M.: Device-free RF human body fall detection and localization in industrial workplaces. IEEE Internet of Things Journal **4**(2), 351–362 (April 2017). https://doi.org/10.1109/JIOT.2016.2624800
8. Mokhtari, G., Zhang, Q., Fazlollahi, A.: Non-wearable UWB sensor to detect falls in smart home environment. In: 2017 IEEE International Conference on Pervasive Computing and Communications Workshops (PerCom Workshops). pp. 274–278 (March 2017). https://doi.org/10.1109/PERCOMW.2017.7917571
9. Palipana, S., Rojas, D., Agrawal, P., Pesch, D.: FallDeFi: Ubiquitous fall detection using commodity Wi-Fi devices. Proc. ACM Interact. Mob. Wearable Ubiquitous Technol. **1**(4), 155:1–155:25 (Jan 2018). https://doi.org/10.1145/3161183, http://doi.acm.org/10.1145/3161183

10. Pätzold, M., Gutiérrez, C.A.: Spectrogram analysis of multipath fading channels under variations of the mobile speed. In: 2016 IEEE 84th Vehicular Technology Conference (VTC-Fall). pp. 1–6 (Sept 2016). https://doi.org/10.1109/VTCFall.2016.7881234
11. Phillips, C., Sicker, D., Grunwald, D.: A survey of wireless path loss prediction and coverage mapping methods. Communications Surveys Tutorials, IEEE **15**(1), 255–270 (2013)
12. Sarkar, T.K., Ji, Z., Kim, K., Medouri, A., Salazar-Palma, M.: A survey of various propagation models for mobile communication. Antennas and Propagation Magazine, IEEE **45**(3), 51–82 (Jun 2003)
13. Stüber, G.: Principles of Mobile Communications. Springer, 3rd edn. (2011)
14. Su, B.Y., Ho, K.C., Rantz, M.J., Skubic, M.: Doppler radar fall activity detection using the wavelet transform. IEEE Transactions on Biomedical Engineering **62**(3), 865–875 (March 2015). https://doi.org/10.1109/TBME.2014.2367038
15. Vasisht, D., Kumar, S., Katabi, D.: Decimeter-level localization with a single WiFi access point. In: 13th USENIX Symposium on Networked Systems Design and Implementation (NSDI 16). pp. 165–178. USENIX Association, Santa Clara, CA (2016), https://www.usenix.org/conference/nsdi16/technical-sessions/presentation/vasisht
16. Wang, W., Liu, A.X., Shahzad, M., Ling, K., Lu, S.: Device-free human activity recognition using commercial WiFi devices. IEEE Journal on Selected Areas in Communications **35**(5), 1118–1131 (May 2017). https://doi.org/10.1109/JSAC.2017.2679658
17. Wang, X., Gao, L., Mao, S.: CSI phase fingerprinting for indoor localization with a deep learning approach. IEEE Internet of Things Journal **3**(6), 1113–1123 (Dec 2016). https://doi.org/10.1109/JIOT.2016.2558659
18. Wang, X., Yang, C., Mao, S.: PhaseBeat: Exploiting CSI phase data for vital sign monitoring with commodity WiFi devices. In: 2017 IEEE 37th International Conference on Distributed Computing Systems (ICDCS). pp. 1230–1239 (June 2017). https://doi.org/10.1109/ICDCS.2017.206
19. Wang, Y., Wu, K., Ni, L.M.: WiFall: Device-free fall detection by wireless networks. IEEE Transactions on Mobile Computing **16**(2), 581–594 (Feb 2017). https://doi.org/10.1109/TMC.2016.2557792
20. Xie, Y., Li, Z., Li, M.: Precise power delay profiling with commodity WiFi. In: Proceedings of the 21st Annual International Conference on Mobile Computing and Networking. pp. 53–64. MobiCom '15, ACM, New York, NY, USA (2015). https://doi.org/10.1145/2789168.2790124, http://doi.acm.org/10.1145/2789168.2790124